Combining numerical tools to determine wave forces on moored ships

Dobrochinski, João P.H.; van Deyzen, Alex; Zijlema, Marcel; van der Hout, Arne

DOI
10.1016/j.coastaleng.2022.104224

Publication date
2023

Document Version
Final published version

Published in
Coastal Engineering

Citation (APA)
Dobrochinski, J. P. H., van Deyzen, A., Zijlema, M., & van der Hout, A. (2023). Combining numerical tools to determine wave forces on moored ships. *Coastal Engineering*, *179*, Article 104224. https://doi.org/10.1016/j.coastaleng.2022.104224

Coastal Engineering 179 (2023) 104224

Contents lists available at ScienceDirect

Coastal Engineering

journal homepage: www.elsevier.com/locate/coastaleng

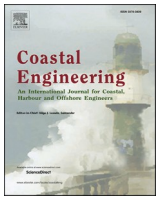

Combining numerical tools to determine wave forces on moored ships

João P.H. Dobrochinski [a,*], Alex van Deyzen [b], Marcel Zijlema [c], Arne van der Hout [a,c]

[a] Deltares, the Netherlands
[b] Royal HaskoningDHV, the Netherlands
[c] Delft University of Technology, the Netherlands

ARTICLE INFO

Keywords:
Mooring
Wave-ship interaction
Waves
Coupling tool
Exposed berths

ABSTRACT

Accurate modelling of waves in harbours and the response of moored ships to that type of forcing is of prime importance to determine the safety and workability of ships moored at berths exposed to local wave conditions. This study investigates the combination of a non-hydrostatic wave-flow model (SWASH) and a 3D boundary-integral diffraction model (Harberth) to compute wave forces acting on moored ships. A series of systematic numerical tests has been performed to develop the proposed methodology and gain insight on its limits of application. The approach is validated using physical scale model test data of waves and forces acting on a restrained ship. Results indicate a good performance even for extremely energetic wave conditions, setting the investigated modelling approach as a potential alternative for future applications.

1. Introduction

The demand for the construction of marine berths at nearshore locations exposed to waves and other loading types is increasing. Moreover, with the increase of ship dimensions, entrance channels to harbours are deepened and widened, making berths possibly even more exposed to the local wave conditions. The resulting wave forces acting on moored ships may induce large motions of the body, which will be transferred to mooring line and fender loads. Under extreme forcing, the ship and mooring structures can be damaged, dangerous line breaking accidents can occur, or the ship movements can be too large to continue the on/off-loading process, resulting in downtime of the berth (PIANC WG 115 (Permanent International Association of Navigation Congresses – PIANC, 2012), PIANC WG 24 (Permanent International Association of Navigation Congresses – Pianc, 1995) and the upcoming PIANC WG 212 (update of WG 24).

Accurate prediction of local wave action and the response of moored vessels is of prime importance to determine safety and workability at berth, as well as to verify the effectiveness of mitigating alternatives. Such an evaluation can follow a three-step approach: (1) determine the wave regime at the mooring location; (2) convert waves into forces and moments acting on the vessel; and (3) calculate the dynamic motion behaviour of the vessel considering the wave-induced forces and the mooring system.

For berths located in coastal regions, determining the wave regime at the mooring site is often the critical step of the approach. This is especially due to the relevance of various nearshore wave transformation processes in combination with complex port geometries and bathymetry. As a result of these (shallow-water) processes, the wave conditions at the mooring site are usually rather different from the incident wave conditions outside the harbour.

In addition to the wave transformation processes, especially in coastal waters the short-wave grouping induces lower-frequency oscillations – the so called infragravity waves with typical periods ranging from 30 to 300 s. Even with relatively small amplitudes, infragravity waves can influence considerably and even dominate the behaviour of moored ships. The low-frequency waves may excite harbour seiches or overlap the frequency of resonance of the ship and mooring system, resulting in amplification of ship motions and mooring loads.

Computational models to assess the wave forcing on moored ships in complex port geometries have been developed over the last decades (see for example (Mynett et al., 1985; Bingham, 2000; Wenneker et al., 2006; Christensen et al., 2008; Rijnsdorp and Zijlema, 2016)). Two established methods have been developed by Van der Molen (Van der Molen, 2006):

a) An infragravity wave model in combination with a strip theory method (Van Der Molen et al., 2006);
b) A Boussinesq-type wave model in combination with a boundary-integral method (Van der Molen and Wenneker, 2008).

* Corresponding author.Boussinesqweg 1, 2629, HV, Delft, the Netherlands.
E-mail address: joao.dobrochinski@Deltares.nl (J.P.H. Dobrochinski).

https://doi.org/10.1016/j.coastaleng.2022.104224
Received 22 December 2020; Received in revised form 17 September 2022; Accepted 25 September 2022
Available online 4 October 2022

In the first method, the wave penetration is calculated using a shallow-water model forced on wave-group scale to calculate the bound and free long waves (Reniers et al., 2004). The approach is computationally effective and adequate in cases where the long-wave propagation is dominant and the high-frequency response can be neglected (this is the case for e.g. berths sufficiently sheltered from short waves but exposed to long waves or harbour oscillations). A similar approach was developed by Deltares and MARIN (Dutch research institutes in the field of coastal and maritime engineering, respectively) for a ship moored in intermediate water depths (Van der Hout et al., 2015), but also for more exposed nearshore terminals including short-wave forcing as well (Jaouën et al., 2016).

Method "b", listed above, uses a Boussinesq-type wave model in combination with a boundary-integral method, which has the advantage that both the high- and low-frequency response of a moored ship can be determined simultaneously. For exposed berths, the high-frequency response (e.g. roll) might be limiting as well. The disadvantage is that the Boussinesq-type wave model may not always be robust for larger wave heights (Van Mierlo, 2014; De Roo et al., 2015).

In the present study, the combination of the non-hydrostatic wave-flow model SWASH (Zijlema et al., 2011) and the 3D diffraction model Harberth (Van der Molen and Wenneker, 2008) is investigated, and a coupling between these numerical models has been developed in order to accurately compute wave forces acting on moored ships in coastal areas (Dobrochinski, 2014). The analysis of the dynamic motion behaviour of the moored vessel is not covered in this study. Nevertheless, once the time series of wave forces and moments is obtained, the simulation of ship motions and loads on mooring lines and fenders is relatively straightforward and several proven methods are available for this, e.g., Quaysim (Van der Molen et al., 2010), AnySim (MARIN), Orcaflex (Orcina), Moses (DNV-GL), Ansys AQWA (Ansys), Ariana (Bureau Veritas).

1.1. SWASH model

Over the last years, the non-linear phase-resolving wave model SWASH, developed at Delft University of Technology, proved its capabilities to reproduce the intermediate and shallow water wave processes relevant for wave penetration studies in ports and harbours (Zijlema and Stelling, 2005; Zijlema et al., 2011; Smit et al., 2013; Rijnsdorp et al., 2014; Rijnsdorp and Zijlema, 2016). The processes simulated by SWASH include non-linearity in the short waves, wave breaking, wave diffraction, wave refraction on variable bed topography, wave interaction with structures (dissipation, reflection, transmission), and infragravity wave generation and transformation. Typical application of SWASH are the simulations of wave transformation in (shallow-water) coastal waters (e.g. breaking zones, swash zones, wetlands).

The SWASH model computes wave transformation by solving the Reynolds-averaged Navier-Stokes equations for an incompressible fluid with a constant density and a free surface. The numerical approach adopted in SWASH is mass and momentum conservative (Zijlema, 2019) and requires much fewer grid cells in the vertical direction for accurate solution than other concurrent methods (e.g. the VOF approach in non-conservative OpenFOAM, developed by OpenCFD Ltd). Further, the applicability range of the model can be extended to larger water depths by simply increasing the number of vertical layers, which is a benefit over most commonly used Boussinesq-type models (see for example (De Jong et al., 2009; De Jong et al., 2011)). The SWASH model version 7.01AB is used in the present study.

1.2. Harberth model

Harberth is a time-domain boundary-integral diffraction model developed at Delft University of Technology, to determine the time-varying wave forces and moments acting on a vessel. The method and implementation are described in (Van der Molen, 2006; Van Der Molen et al., 2006; Van der Molen and Wenneker, 2008), although the software name 'Harberth' came in use after these publications. The interactions between the body and the surrounding fluid are computed by Harberth based on linear potential theory, superposing the potentials due to the undisturbed incoming wave, the scattered/diffracted wave, and the radiated waves induced by the body motions.

The undisturbed incident wave is prescribed at collocation points along the ship's hull as input to Harberth. The normal velocities on the hull serve as boundary condition for the boundary-integral model for the scattered waves, while velocities along the hull are required for the determination of the second-order forces. The incident wave pressures are used for the determination of the wave forces, and incident wave elevations prescribed at the waterline segments are employed in the computation of the second-order forces. The undisturbed incident wave can, for example, be based on linear wave theory or can be calculated with a (typically nonlinear) external wave model (i.e. SWASH in this case).

The scattered waves due to the diffraction of the incident waves by the ship and the radiated waves due to the motions of the ship are computed by Harberth using a linear 3D panel-based time-domain diffraction model. The integration of the wave pressures over the submerged hull of the ship provides the corresponding first- and second-order forces and moments.

The first-order wave exciting forces and moments are obtained by linearly superposing the Froude-Krylov force and the diffraction force, associated with the incident (undisturbed) waves and the scattered waves, respectively. The second-order wave drift forces are determined using the near-field pressure integration method from the product of calculated first-order quantities (i.e., incident, scattered and radiated waves, and ship motions due to 1st order forces). The integration of the pressure due to the radiated potentials provides the hydrodynamic coefficients and retardation functions used to compute the vessel motions.

1.3. Objective of the study

The objective of the present study is to combine the SWASH wave model and the Harberth model to accurately compute wave forces acting on moored ships. A tool to convert the SWASH model results into the Harberth model input, referred to in the remainder as the *coupling tool*, has been developed. The technical background of this coupling and its verification based on scale model test results are described in this paper. The presented research is aimed to investigate to which extent the combined tools can simulate conditions that are relevant for harbour applications, verifying its accuracy and effectiveness. Additionally, the contribution of each component of the approach to the accuracy of the end results is evaluated, therewith providing guidance and recommendations for future practical applications related to port designs and optimisations.

Though the methodology of combining a phase-resolving wave model with a 3D boundary-integral diffraction model to compute wave loads on moored ships has been known to reach a matured level, the novelty of the proposed approach can be summarized as follows.

- The introduction of the SWASH wave model to the modelling chain constitutes the main innovation as outlined in this paper, given the robustness of SWASH under extreme wave heights – under which well-established Boussinesq-type wave models are occasionally robust (Van Mierlo, 2014; De Roo et al., 2015). Further (Van der Hout et al., 2015), indicates limitations of operational (low-order) Boussinesq-type models to simulate bound long waves at the intermediate depths relevant for nearshore mooring terminals.
- Development of a coupling procedure between a wave model with vertical resolution and a 3D boundary-integral diffraction model. The sensitivity of the number of vertical layers in the wave model and vertical interpolation strategies of model results is assessed under various wave conditions, identifying the coupling

performance and the potential introduction of errors or additional requirements to the overall model approach. As a note, the investigated coupling procedure has conceptual differences when compared with common approaches using, e.g., Boussinesq-type models (Wenneker et al., 2006; Van der Molen and Wenneker, 2008). These are especially related to the differences in the vertical discretization between the wave modelling paradigms.

- Evaluation of amplitude and phase errors in the SWASH wave model considering different wave conditions, variations in the horizontal and vertical grid resolution, and different sets of numerical schemes. Similar assessments have not been documented yet. They can provide basis for model optimization, while also highlighting for expected errors and limitations in the wave computations that may negatively affect results of wave penetration and mooring studies.
- The specific combination of SWASH and Harberth via the developed coupling tool has not been tested or verified yet. The validation of the approach against measurements provides insight on the accuracy level, highlights for potential sources of errors and limitations, and therefore provides basis for practical engineering applications.

The rest of the paper is organized as follows. Section 2 presents the development of the approach by considering a large set of simplified wave conditions. For these initial tests more elementary results are found, enabling an insightful analysis of the performance of the applied tools. Following the initial verifications, in Section 3, the approach is validated using physical scale model tests of a captively moored vessel in realistic wave conditions (WL | Delft Hydraulics (2004) – presently Deltares), demonstrating the possibility of employing the proposed computation approach in practical engineering applications. Lastly, the main findings are summarized along with concluding remarks in Section 4.

2. Model preparation

This section presents a general assessment of the applicability of SWASH considering different model settings and various regular wave conditions (Section 2.1). Section 2.2 describes the development of the *coupling tool* to convert SWASH model results into Harberth input files. The computed hydrodynamic loads are assessed in order to check the overall consistency of the proposed approach, as well as its accuracy and possible limits of application (Section 2.3).

2.1. Wave modelling with SWASH

The accuracy of the computed wave forces acting on a moored vessel is linked to the accuracy of the local wave computations, which – for a given numerical wave model (type) – generally improves by reducing grid size and time step at the expense of larger computational time. As the wave modelling typically represents the most time-demanding step of ship mooring analysis applications at coastal areas with complex geometry, a good understanding of the trade-off between accuracy and computational time is deemed necessary. This remarkably applies in practical port engineering tasks, where several tens or hundreds of such analyses need to be made.

The computational effort associated to the wave modelling in SWASH is proportional to the number of vertical layers and inversely related to the grid spacing and time step. The SWASH model automatically adjusts the time step to keep the Courant number sufficiently low and ensure numerical stability. As the adopted time step is shorter for finer grid spacing, the computational effort relates to the horizontal spacing to the power three (i.e. dx, dy, dt). Therefore, the horizontal resolution represents a rather critical definition with respect to the required computational time of practical applications. However, the relations between horizontal spacing and the SWASH model accuracy for various wave conditions is not yet objectively defined for the purposes of computing wave forces on floating bodies.

A series of 288 systematic tests considering different model settings and regular waves with distinct characteristics has been performed with SWASH to evaluate the relations between the modelled wave conditions, numerical model definitions, and the expected accuracy of the results. The tests are executed in 2DV mode (i.e. line domain or x-z plane) considering a flat bottom (20 m deep) without bottom friction:

- wave periods: 18s; 10s; 5.2s; 4s ($kd = 0.5$, 1, 3 and 5, respectively).
- wave heights: 0.01m; 1m; 2m ($ak < 0.25$).
- horizontal resolutions [grid points/wave length]: 100; 40; 20; 10.
- vertical resolutions [number of equidistant vertical layers]: 20; 3; 2.
- sets of numerical advection schemes: *default* set; *adapted* set.

with $k = 2\pi/L$ the wave number, d the water depth, L the wave length and a the wave amplitude. To further understand the modelled wave conditions regarding non-linearity and relation with the maximum stable wave height, the tested cases are plotted along with Fenton's parameterized relation of the Williams points (Fenton et al., 1990) (Fig. 1). The degree of non-linearity of the regular wave conditions is indicated using the 'Stokes Ratio', which is the ratio between the free-surface amplitude of the second-order Stokes correction to the primary wave amplitude.

The simulated wave conditions lay within the 'plot-area' where the Stokes Theory is most suitable: waves which are not very long relative to the water depth. Following the Stokes Ratio metric (S), the non-linearity is maximum for the test condition with wave height of 2 m and wave period of 18 s (S = 0.17), followed by the test condition with wave height of 2 m and wave period of 4 s (S = 0.13).

The tested sets of numerical discretization schemes applied for the advection terms in the momentum equations are listed in Table 1. A distinction is made between the advection contributions of the u-momentum equation and the w-momentum equation, with u and w the horizontal and vertical velocity component, respectively. Each equation includes two terms of momentum advection (see first column of Table 1; H: horizontal, V: vertical). For details, see (Zijlema et al., 2011).

Various discretization schemes applied to momentum advection have been developed, of which the common ones are (see also Table 1): the first order upwind scheme (UPW), the second order upwind scheme (BDF) and the second order central difference scheme (CDS). Further details can be found in (Hirsch, 1990). The combination of schemes to be used in SWASH depends on the type of application and situation considered.

The *default* set (middle column of Table 1) is suitable for low-to mid-frequency wave transformation in coastal waters (say $kd < 1$), whereas the energy of shorter components will have been dissipated by wave breaking. However, in deeper waters that typically occur at harbours and mooring locations such shorter ($1 < kd < 3$) components may still be relevant (e.g., for the high-frequency response of a moored vessel or as the forcing to infragravity waves). In such intermediate water cases and especially under non-linear wave conditions – typical in harbour applications, enforcing the momentum conservation and choosing a higher-order scheme for the vertical advection of u-momentum is preferable. For this reason, the *adapted* set (right column of Table 1) is included in the tests described in this paper. The modification of the schemes in horizontal momentum equations should not increase the computational time because the computational stencil remains the same. The advective terms of the vertical-momentum equation are usually small compared to the vertical acceleration in water of shallow and intermediate depths and can thus be safely ignored (Zijlema et al., 2011). This has been confirmed for the testing conditions described in this section.

Following recommendations in the SWASH model user manual, the discretization of the vertical pressure gradient uses the classical central differencing scheme employing the standard layout for the simulation with 20 vertical layers. The simulations with 3 and 2 vertical layers use the implicit Keller-box scheme. Because of that, different convergence

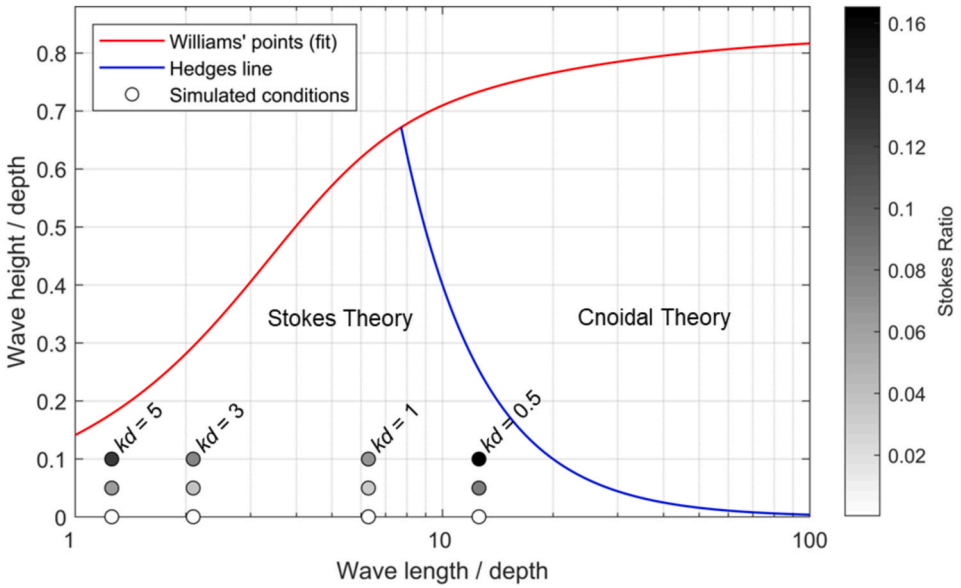

Fig. 1. Test conditions relative to the regions in which solutions for steady waves can be obtained. The empirical curve (red) represents Williams' experimental points for the highest waves. Hedges' proposed demarcation line (blue) between Stokes and Cnoidal theories.

Table 1
Discretization of advection terms in the momentum equations. BDF: 2nd order Backward Difference Scheme; CDS: 2nd order Central Difference Scheme; UPW: 1st order Upwind Scheme. In addition, momentum conservation is enforced in the Adapted set of schemes.

	Term	Default set	Adapted set
$u\frac{\partial u}{\partial x}$	(H. Adv. of u-momentum)	BDF	BDF
$w\frac{\partial u}{\partial z}$	(V. Adv. of u-momentum)	UPW	CDS
$u\frac{\partial w}{\partial x}$	(H. Adv. of w-momentum)	Ignored	Ignored
$w\frac{\partial w}{\partial z}$	(V. Adv. of w-momentum)	Ignored	Ignored

rates between the two cases should be expected when analysing results.

When judging wave model outcomes, both the wave amplitudes and the wave phases are relevant. Even more so in case of applications involving moored vessels, since both the magnitude and timing of forcings will be critical. Therefore, phase/dispersion and amplitude errors are calculated from the results of the 288 tests considering regular waves (see scheme in Fig. 2). The dispersion errors correspond to deviations between the wave celerity computed with SWASH and analytical results for a flat bottom situation calculated using stream function theory and based on the nonlinear spectral approach discussed in (Fenton et al., 1990) and implemented in the program *Fourier* by Prof. John Fenton (see https://johndfenton.com/Steady-waves/Fourier.html). For the tested conditions these differences are generally smaller than 1% of the analytical wave celerity for the longer wave conditions ($kd \leq 1$) and 2% for $kd = 3$, which is deemed negligible in practice for studies of wave penetration in harbours. Larger errors in the order of 5% are encountered for the shorter wave condition considered in the tests ($kd = 5$). If necessary, these can be reduced with using more vertical layers (>3 layers) and taking into account the advection terms of w-momentum.

The amplitude errors correspond to a deviation of the regular wave height along the wave propagation directions across the computational domain, and occur as: 1) a drop in wave height within the first wave length from the model boundary, and 2) as a gradual decay along the domain (i.e. numerical dissipation; notice that bottom friction is neglected in these fundamental tests) (Fig. 3).

The amplitude errors near the boundary are negligible for longer waves (kd $\leq$ 1) but can become significant for relatively short waves (~5% for $kd = 3$; 10–20% for $kd = 5$). These errorsare only slightly affected by the imposed wave height, horizontal/vertical resolution and numerical schemes. These errors are attributed to limitations in prescribing highly hyperbolic boundary conditions.

SWASH applies the linear wave theory to generate free waves at the wavemaker, with the addition of second order correction for the bound waves (Hasselmann,1962) – not relevant in the tests with regular waves. Because super harmonics are not included in the numerical wave maker of SWASH (version 7.01AB), spurious free waves with the frequency of the super harmonics may be introduced in the incoming boundary. The amplitude of the spurious waves is approximately the free-surface amplitude of the second-order Stokes correction (within the validity of the Stokes Theory, see Fig. 1). If the wave conditions at the boundary are weakly non-linear, the spurious higher-frequency waves are expected to be small and not significantly influence the overall model results. Otherwise, the effects need to be taken into consideration in the modelling work.

According to the linear wave theory both the u-component and the w-component have a cosine-hyperbolic profile over the vertical. However, as presently implemented in SWASH, only the u-component is imposed with a cosine-hyperbolic profile based on the boundary condition, and not the w-component. If the advection term of w-momentum is taken into account in the simulation, a Neumann condition is applied at the wavemaker meaning that the flux $dw/dx = 0$ at the boundary. This is not intended to reduce errors, and thus have a marginal or slight negative effects on the amplitude errors near the boundary. The overall approach used by the wave generation machinery in SWASH has been reasoned from the view of coastal engineering, and is acceptable if the variation of w (and also u via the mass balance) over the vertical is not too strong ($kd < 3$).

The numerical dissipation is negligible for linear waves ($H = 0.01$m, not shown here), but can become significant for short non-linear conditions ($kd > 1$, $H = 2$m). These errors relate to the way SWASH handles the vertical advection of u-momentum and the enforcement of momentum conservation (vs. energy head), and can be reduced to negligible levels by using the *adapted* set of numerical schemes, provided that the horizontal model grid resolution is sufficient (>10 grid points per wave length).

Summarizing, the results of the systematic tests indicate that the

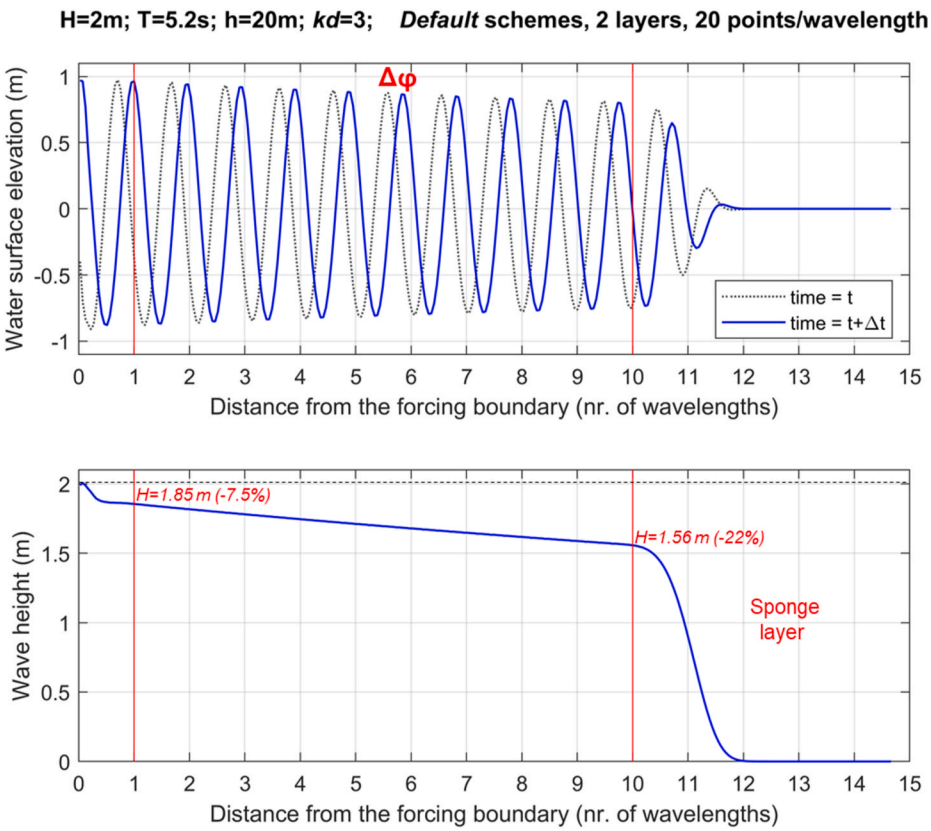

Fig. 2. Schematic view of the computed errors from SWASH simulations considering regular waves. This example is associated with the test condition H = 2m, kd = 3, *Default schemes*, 2 vertical layers and 20 grid points per wave length. Upper panel: dispersion errors ($\Delta\varphi$ is the wave phase displacement during a timestep Δt; $\Delta\varphi/\Delta t$ = wave celerity); lower panel: amplitude errors. Waves are imposed in the 'left' boundary; a sponge layer is included in the opposite side to avoid reflected waves.

amplitude errors are only marginally affected by using a fairly low number of vertical layers in the SWASH model, so using two layers appears to be sufficient for general coastal applications. Tests using one single layer are not included in this paper, as this setting is insufficient for wave components that are typically relevant in harbour applications ($kd > 1$). Nevertheless, in specific (shallow-water) cases where such wave components can be neglected, using one vertical layer may be an option for improved computational performance. However, considering the physical complications within harbours (e.g., nonlinearities, shoaling, refraction in steep slopes, diffraction, wave-wave interaction, reflection), sensitivity testing against simulations with two or more layers is recommended.

A horizontal resolution of 20 grid points per wave length suffices for accurate results. Near-boundary amplitude errors is negligible for ($kd \leq 1$) and increase gradually for shorter-wave components ($kd > 1$), which are usually of less importance for practical finite-depth applications. In case such shorter-wave components are important, as a practical solution the imposed spectra may be amplified in order to overcome the observed energy drop. In this case, the amplification factor should be frequency-dependent (i.e. focused on the higher-frequency components), therewith avoiding an over estimation of lower frequency energy in the simulations. The numerical dissipation along the domain can be especially critical for non-linear and relatively short waves ($kd > 1$). If those wave components are important, the *adapted* set of schemes should be used to suppress these errors, otherwise the *default* set of schemes may be an option for increased robustness.

Although the ability of SWASH to prescribe short-waves ($kd > 3$) at the boundary has been recently extended through using internal wave generation techniques (Vasarmidis et al., 2019, 2021), this implementation is presently only available for regular grids and thus impractical for engineering applications. Further, such short waves are arguably irrelevant in most harbour and coastal mooring applications, which typical deal with mid-to long-period energetic wave conditions (peak period $T_p > 10$ s) at water depths in the order of 20 m or less. Under such conditions, the shorter-wave components with $kd \geq 3$ correspond to the less relevant tail of the wave spectra ($f > 2*f_p$). Considering that and the results presented in this Section, provided that the model settings are adequate SWASH is deemed sufficiently accurate for simulating the wave conditions that are typically relevant for harbour applications.

2.2. Development of the coupling tool

As introduced in Section 1, a program referred to as the *coupling tool* was developed to read the output files of SWASH, allocate the time-dependent wave quantities at predefined locations along the hull of the ship (3-dimensional dynamic pressure, u, v and w velocity components, and water level), and write the Harberth model input files (Fig. 4).

The high horizontal and temporal resolution of the SWASH results (~4m, ~1s) relative to the spatial and temporal scales of the ship and of the computation (~300m, ~2 h) imposes challenges in terms of computer memory and interpolation time. To facilitate the coupling procedure, the interpolation of the SWASH model results to the collocation points (x_{hull}, y_{hull}, z_{hull}, of each boundary panel describing the hull of the vessel in Harberth) is divided into two steps.

First, the four wave model grid points surrounding each collocation point are identified, and the depth-dependent wave quantities are interpolated to the level of the collocation point z_{hull}. The wave pressure and the vertical velocity component are provided by SWASH at the edge of the layers, and these results are linearly interpolated along the

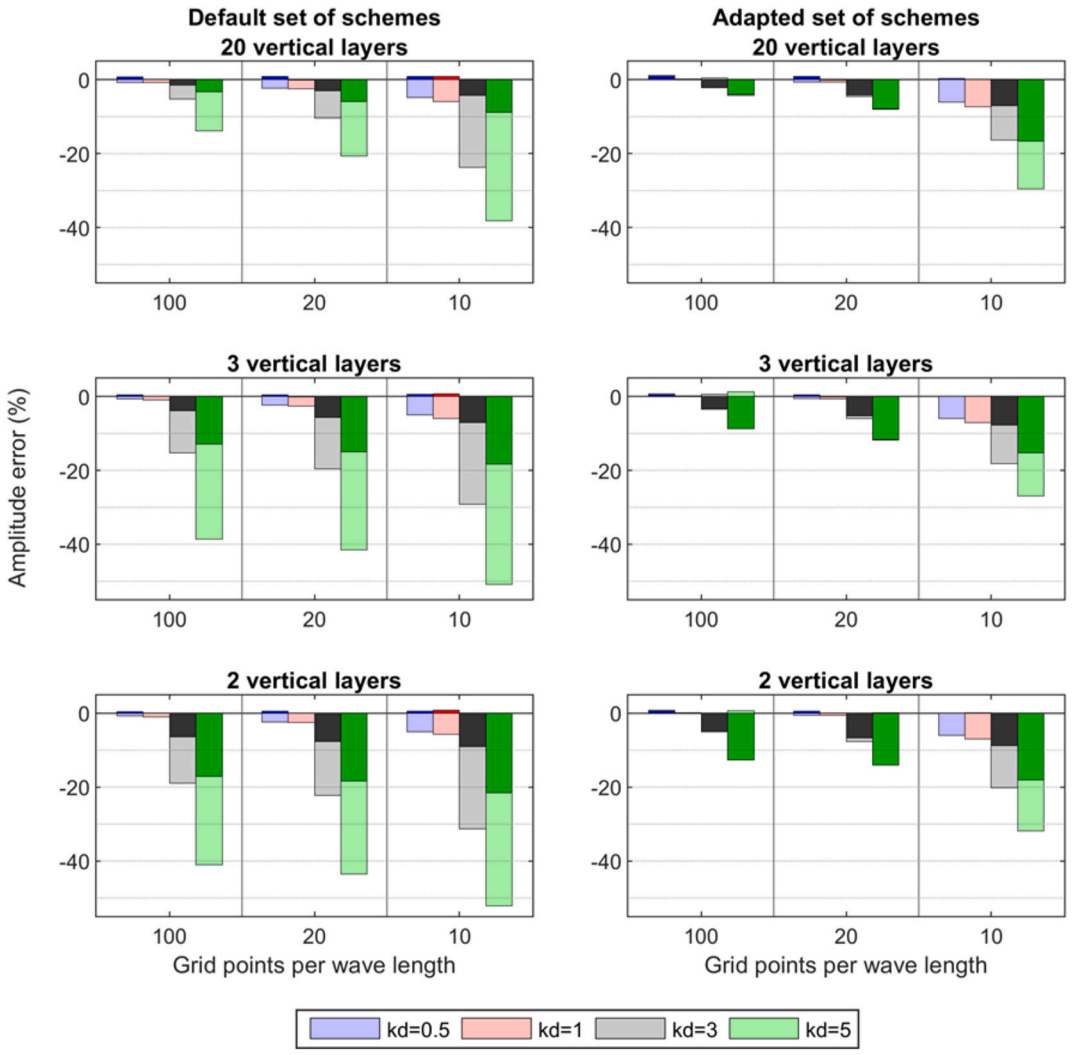

Fig. 3. Amplitude errors (H = 2m), *default* (left) and *adapted* (right) set of schemes. Darker colors: error near the boundary; lighter colors: numerical dissipation after 10 wave lengths.

vertical to determine the input value at the required level. The horizontal velocity components, however, are given in the middle of the vertical layer – whereas velocity information is also required in the coupling to the vessel in the upper half of the surface layer and in the lower half of the bottom layer. Especially when only a few vertical layers are used in the wave model, different interpolation choices to overcome that restraint may lead to variations in the interpolated vertical profiles. Two approximations were considered for the definition of the horizontal velocity components at the required vertical level: 1) vertically uniform horizontal velocity components within each layer; and 2) linearly varying horizontal velocity components within each layer. The slope (dU/dz) of each layer is the average between the slopes at the upper and lower interfaces, which are derived from the model results. At the interface with the bottom the slope is considered to be null (dU/dz = 0), and at the surface it is determined by extrapolating the profile curvature. The two approaches resulted in similar outcomes for shallower and deeper water conditions (kd = 0.5 to 5), although the specific comparison graphics are not included in this paper. For the sake of simplicity, the layer-constant method was selected for the applications described in the following sections.

Following the vertical interpolation to the level of the collocation point (z_{hull}), the information of the four surrounding points is interpolated to the horizontal position of the collocation point (x_{hull}, y_{hull}). Given that several grid points per wave length are required to model the waves, output differences between neighbouring grid points are relatively small. Therefore, for computation efficiency the horizontal interpolation is done using a simple inverse distance-squared weighting method.

Results obtained with the interpolation procedure implemented in the *coupling tool* are generally consistent with the outcomes of fully 3D interpolation functions available in MATLAB®. However, by employing only 1D and 2D interpolation, the alternative approach reduces calculation times considerably.

Lastly, the time-dependent information at the required locations is converted into the Harberth model input files.

In the developed method, results of one SWASH run can be used to compute ship response for different mooring orientations and mooring line configurations. In this regard, the adopted approach of coupling two separate models (i.e., a wave model without the presence of a ship and a ship model) may be beneficial compared to a one complete model integrally modeling the vessel in the computation, that has to be rerun for each different mooring configuration or loading condition. This is especially relevant here, since the wave model is usually the most time-consuming component of the model train for assessing moored vessels under wave loadings.

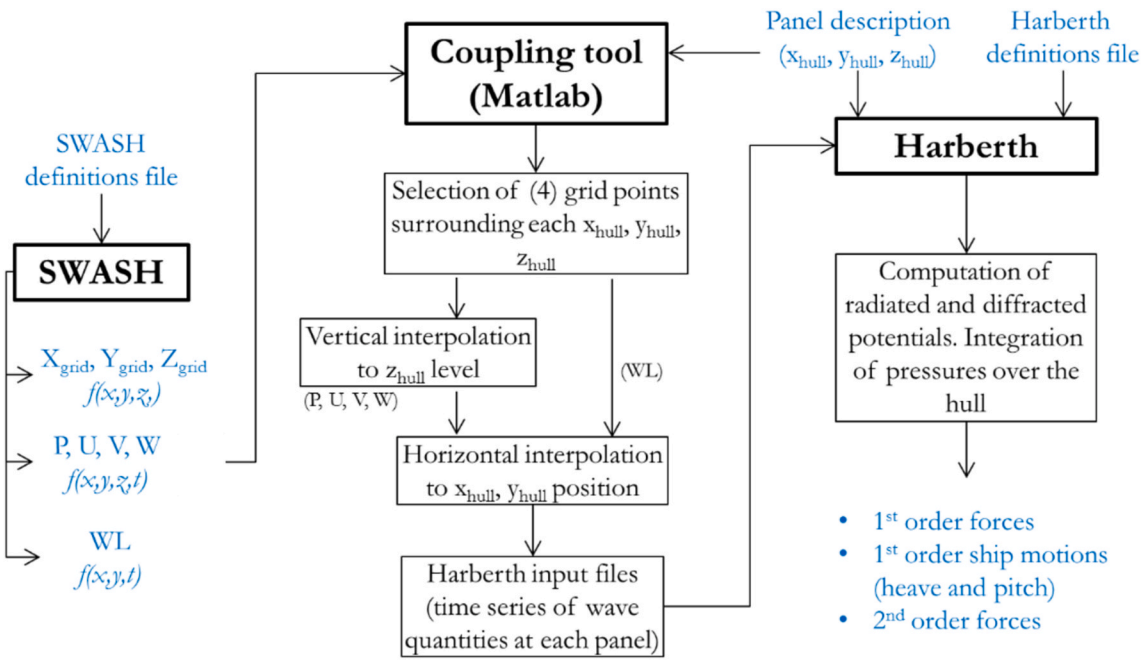

Fig. 4. Flowchart with information (blue) and processes (black) relations within the coupling procedure.

2.3. Computation of wave forces with Harberth

To verify the consistency of the developed *coupling tool* and identify possible application limits, the SWASH model results for the systematic tests with regular waves (Section 2.1) are used as input to the Harberth model in order to compute wave forces acting on a 125,000 m^3 LNG carrier in 20 m water depth. The specific wave tests used in this verification include the four wave periods considered in Section 2.1 (18s, 10s, 5.2s and 4s); a wave height of $H = 0.01$m; 100 grid points per wavelength; 20, 3 and 2 vertical layers; and the *default* set of schemes. The regular-wave direction is considered to reach the ship at 225° relative to the body-bound coordinate system (i.e., bow-quartering wave).

The outputs from the Harberth simulations are time series of wave forces and moments acting on the ship. For regular waves, the variation of the forces and moments becomes cyclic after some time into simulation, once the computational area has 'filled' with wave energy. The amplitudes of the cyclic variations are verified against results obtained with the established frequency-domain 3D panel model Wavescat (Van der Molen, 2011; Van der Molen et al., 2019). The results of the Wavescat model consist of transfer functions relating the incident wave amplitude to the associated forces for a range of exciting frequencies.

The physics behind the Wavescat model are generally similar to the Harberth model (Section 1.2), however Wavescat performs computations in the frequency-domain using linear wave theory to define also the incident wave potentials, so non-linear wave processes relevant for coastal applications are neglected in the Wavescat model. Since the effects of non-linearities are expected to be minimal for the test with regular waves with small amplitudes ($H = 0.01$m), the comparisons are viable and insightful. The total first- and second-order wave forces and moments computed with the proposed methodology (SWASH + *coupling tool* + Harberth) are compared with the Wavescat model results in Fig. 5 and Fig. 6, respectively.

The *first-order* wave forces and moments computed with the proposed method are in satisfactory agreement with Wavescat model results for the tested conditions (Fig. 5), with differences less than 10% for the main wave frequencies. This indicates that the coupling procedure is consistently implemented in the developed tool, and that two vertical layers in SWASH suffice for a proper determination of the wave forces under these testing conditions.

The horizontal modes of *second-order* drift forces and moments computed with the proposed approach are compared with Wavescat results in Fig. 6. In Harberth the contribution of the first-order horizontal displacements is neglected in the computation of the drift force (i.e., the ship is kept captive and is allowed only to heave, roll and pitch). For Wavescat, two sets of results are given: considering all the motion modes (6-DOF), and captive – as in Harberth.

The drift forces computed with the proposed approach are generally in good agreement with the Wavescat model results for the tested conditions. Overall, the differences between Harberth and the (captive) Wavescat results are in the same order as reported in (Naciri and Sergent, 2009), which compares drift forces computed for a single ship and mesh using seven leading commercial diffraction/radiation software.

A more significant difference is reported for the lower-frequency (T = 18 s, ω = 0.35 rad/s) yaw moment (M_z). By comparing the individual terms of second-order forces, this difference is found to be associated with the 'relative wave elevation term' (Term 1) that accounts for the water surface elevation and the first order vertical body motions at the waterline contour along the hull. The water surface elevations are consistent, therefore the differences are attributed to an offset in the phase of the roll motions (~25°) and a slightly (~6%) difference in the amplitude of pitch motions between the results of the two models. These differences become more pronounced in the drift force results because the forces are quadratic (i.e., vertical motions squared). Further, the contributions from Term 1 and Terms 3 and 4 to the yaw moment (M_z) drift force have opposite signs and partly cancel each other at this lower frequency forcing (as a note, the contribution of Term 2 is negligible in this case). Thus, the relative difference in the Term 1 (~20%) becomes greater in the total drift force results (~40%).

Notably, the referred condition (T = 18 s) is near the roll natural frequency. Differences in lower-frequency roll motions computed by Harberth and another model are also reported in (Van der Molen, 2006), where it is stated that roll motions are very sensitive to the calculated phase angles of the roll and sway forces, and that the neglected influence of viscous damping should be included when dealing with large roll motions that are hardly damped by the small radiation damping.

The results of drift forces computed with SWASH + Harberth (20, 3 and 2 layers) deviate at the higher frequencies (T = 5.2 and 4 s; ω = 1.21 and 1.57 rad/s). These differences are mainly associated with the

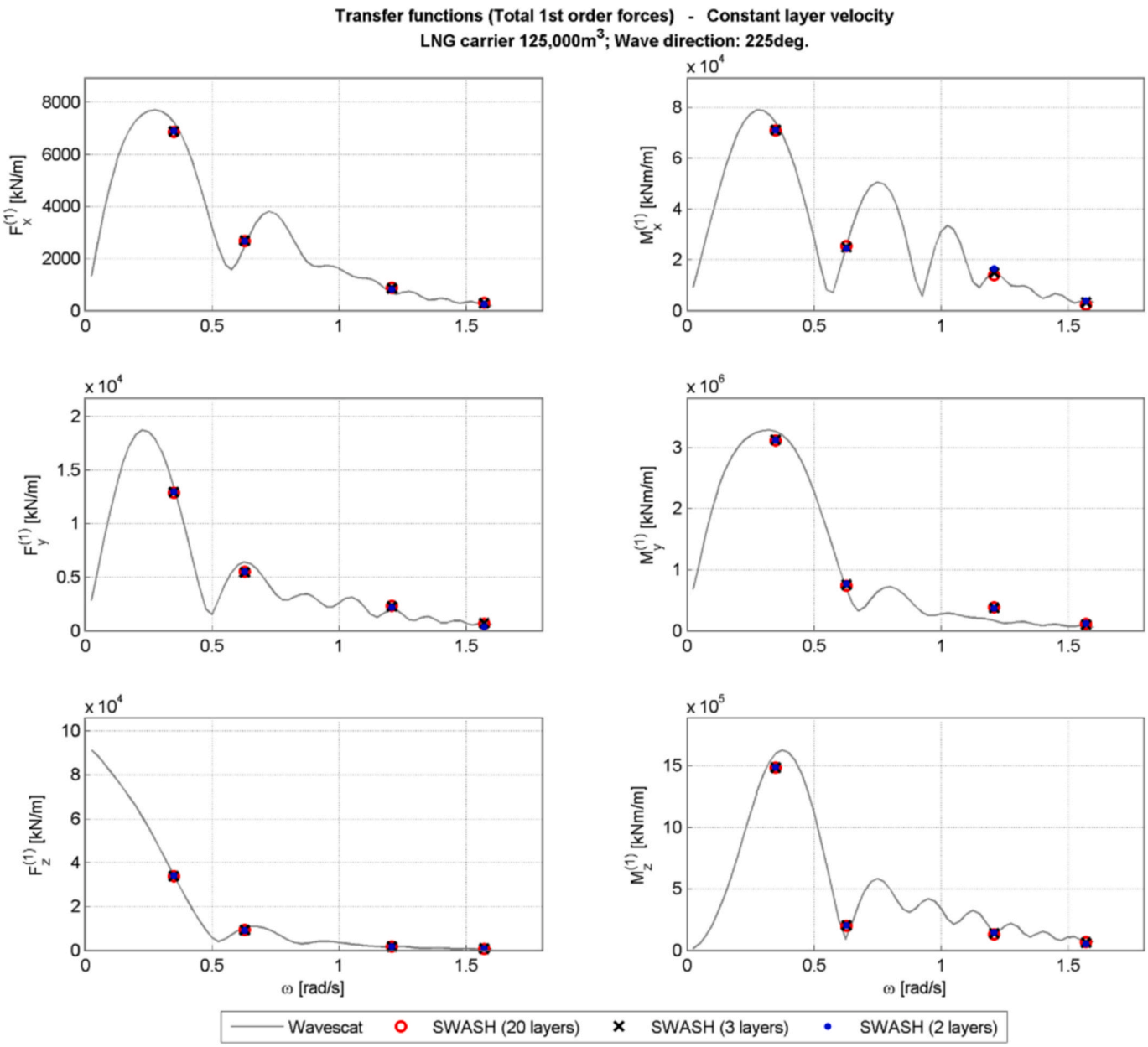

Fig. 5. Total first-order wave forces and moments computed with SWASH + *coupling tool* + Harberth and Wavescat model.

'relative wave elevation term' of the drift forces (i.e., Term 1), and to a lesser extent with the 'second order pressure term' (i.e., Term 2). The other terms (Term 3 and 4) are linked to the body motions, which are rather small at such high frequencies and result in negligible contributions to the drift forces in all simulations.

Although the incident wave elevation can be represented by SWASH using 3 and 2 layers, the curved vertical velocity profile for these deeper water conditions ($kd = 3$ and 5) is coarsely discretized. This leads to inaccuracies in the inputs to Harberth simulations, which reflect in the representation of the diffracted wave (Term 1) and in the second order pressure (Term 2). The effects are amplified in the drift forces as all contributions are quadratic. Further, the contributions from Term 1 and Term 2 to the total drift forces have opposite signs, so the relative differences in the end results are greater. These outcomes indicate that, in applications where such short waves are anticipated to be relevant for the 1st order forces, vessel motions and drift forces, more layers are needed in SWASH to properly prescribe the vertical profiles of incident waves along the ship hull.

The contribution of first-order horizontal displacements (and the captive approximation) appears to be relatively small for the surge and sway drift forces. This is not the case for the yaw drift forces and thus the simplified motions in Harberth have larger effects. This must be taken into account in applications where the first-order waves and the associated surge, sway and yaw motions are significant. However, especially in harbour applications the incident waves and (moored) ship motions are usually smaller, as well as the associated second-order forces. In coastal waters, the low-frequency loads will be likely dominated by incident low-frequency waves, which are properly included in the non-linear wave model and imposed to Harberth as part of the incident waves. Although typically generated by non-linear processes simulated in SWASH, within Harberth these are long and small amplitude waves that will primarily result in corresponding first-order forces in the developed methodology.

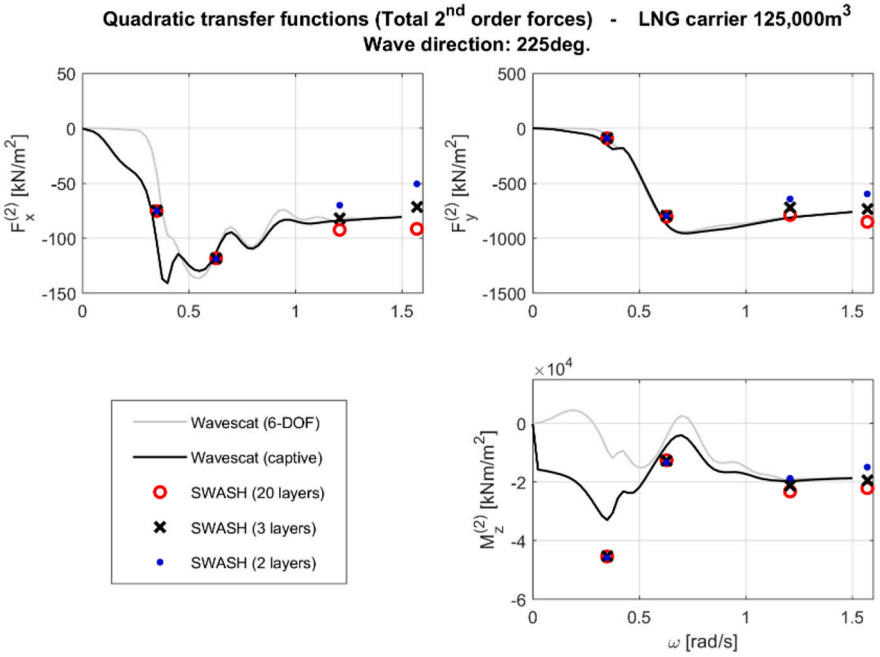

Fig. 6. Total second-order mean drift forces and moments computed with SWASH + *coupling tool* + Harberth and Wavescat model.

3. Validation of the approach

The applicability of the coupling tool was validated against results of physical scale model tests conducted at WL | Delft Hydraulics (now Deltares) in 2004 (Hydraulics, 2004; Van der Molen, 2006). The tested conditions consist of regular, irregular long-crested and irregular short-crested waves, modelled with a uniform water depth of 20m. The measured datasets include waves at different locations in the basin and the forces and moments acting on a restrained Panamax container vessel (length x beam x draft = 255 × 32.26 × 12.00m) at a model scale of 1:100. The ship was fixed to its position by a large steel frame. Six force transducers were fitted in this frame to measure the forces on the ship in the six degrees of freedom. The ship is located in either open water or in a schematic harbour basin, depending on the test series considered.

Fig. 7 shows the layout of the tests, with the wave maker on the left side and rubble mound slopes on the opposing side to minimize wave reflection. The wave maker in the basin enables wave generation in different directions, including the second order long waves to avoid the generation of spurious long waves, and is equipped with active reflection compensation to absorb waves reflected from the basin walls (Van Dongeren et al., 2001).

The wave conditions considered for the validation of the studied approach are listed in Table 2. For the spectral forcing, JONSWAP spectra with peak enhancement factor of $\gamma = 3.3$ are used in both the physical and numerical wave makers. The wave conditions are simulated for 3 h for a proper determination of the waves and forces spectra.

In both tests, the ship is located at the centre of the basin (position GRSM in Fig. 7), making an angle of 120° with the adopted coordinate system. The harbour layout in Test B (top panel of Fig. 7) is composed by vertical impermeable walls (i.e. quay walls) with internal dimensions of 1 200 × 400 m (prototype scale). The ship is located in the middle of the longer wall. It is positioned parallel to the wall, and the ship's midpoint is 20 m (prototype scale) away from the 'quay'. This results in a gap between the ship and the wall of approximately 4 m.

To prevent excessive wave reflection against the vertical side wall, the wave paddles close to the wall were not used in the tests with oblique wave direction (Test B, Dir = 30°). However, the exact length of the wave maker section switched-off in the test was not recorded, so the section applied in the numerical modelling had to be inferred.

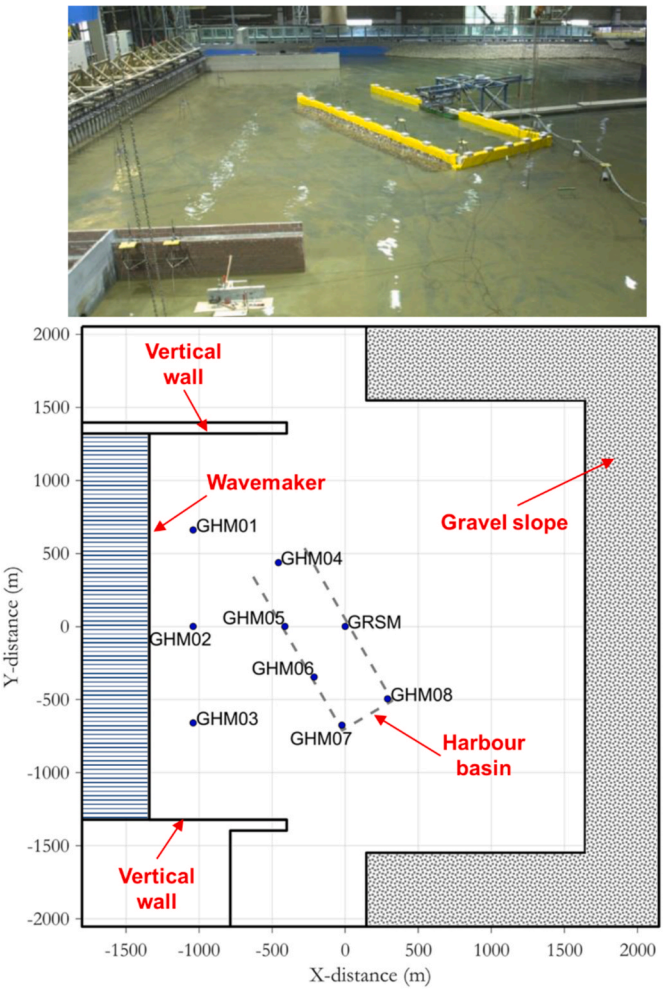

Fig. 7. Layout of the test basin. The midpoint of the ship is the origin of the coordinate system ($X = 0$m, $Y = 0$m).

Table 2
Wave conditions (full-scale) in the validation of the approach (wave directions relative to the *x*-axis, see Fig. 7). Hs is the significant wave height, Tp is the wave peak period and Dir is the mean wave direction. The numbers in brackets are the original identification tests of WL | Delft Hydraulics (Hydraulics, 2004; Van der Molen, 2006).

Test	Hs	Tp	Dir	Directional	Ship
	[m]	[s]	[°]	Spreading	Position
A (2.3.1.2)	1.5	10	0	$\cos^2$	Open water
B (4.3.3.2)	6	15	30	$\cos^4$	Harbour basin

Experiment and numerical model results are compared using frequency spectra and spectral parameters derived from raw/unfiltered measured and simulated timeseries of water surface elevation, forces, and moments. The initial 12 min are excluded from both the measured and simulated time series to prevent the influence of the initial conditions in the analysis.

For reference, the model-data agreement presented in the next sections can be qualified as follows: measures <15% are considered good, measures between 15% and 30% indicate reasonable agreement, and measures >30% indicate significant discrepancies.

3.1. Wave modelling

The SWASH wave model was configured to represent the test basin. The computational grid has two equidistant vertical layers and 707 × 803 computational points over the horizontal space, giving a maximum resolution of approximately 4 × 4 m^2 in the region between the wave maker and the harbour and ship location. This resolution corresponds to approximately 30 grid points per wave length for a wave component with T = 10 s in 20 m water depth; and approximately 10 grid points per wave length for a wave component with T = 5 s. The effects of this coarser representation are expected to be marginal, as the higher frequency wave components relate to the less energetic tail of the wave spectra and are short relative to the size of the ship. The wave computations were 3 h long, and the associated computation times were in the order of 1.5 days (running in parallel using 12 conventional computational cores).

The vertical side walls near the wave maker, surrounding the harbour (Test B) and the gravel slopes are included in the computations as porous structures. (Partial) reflection, dissipation and transmission through structures are determined by SWASH based on the structural porosity and the diameter of the granular material (d_{50}). The porosity of the vertical walls is defined as zero (i.e. impermeable), whereas $p = 0.45$ is used for the side slopes. The d_{50} of both structures is 2 m. The *adapted* set of numerical schemes is applied to reduce numerical dissipation. For Test A the bottom friction coefficient is calculated using the Manning formula with a coefficient of 0.019 $m^{1/3}s$, which gives $c_f = 0.0013$ at 20 m water depth.

Energy dissipation due to bottom friction is important for representing the seiching modes and resonance in the harbour basin. Hughes (1993) reports that scaling effects on turbulence/viscosity can make bottom friction in the model tests significantly greater than in prototype. Sensitivity tests with different quadratic bottom friction coefficients were carried out for Test B. The value $c_f = 0.03$ provided satisfactory results for both short and long waves in the harbour basin.

Measured and simulated wave spectra for tests A and B are given in Fig. 8 and Fig. 10, respectively. The snapshots of the simulated water surface elevation and significant wave height for Test B (Fig. 9) give a general impression of the SWASH model results. The lower panel in Fig. 9 indicates a non-uniform distribution of wave heights within the harbour basin as a result of wave reflection and standing wave patterns. This is also present at the location of the ship, where the significant wave height varies from approximately 2.8 m along on the portside of the ship to 4.5 m closer to the wall, within a distance of approximately 30 m.

For the test condition A, the *kd* values of wave components at peak frequencies is approximately $kd_{peak} = 1$, while higher-frequency components (e.g., twice the peak frequency) have an associated $kd_{2fp} = 3.2$. The degree of non-linearity measured by the Stokes Ratio (Section 2.1) is in the order of S = 7%, considering that high individual waves have typically the peak period and 1.5 times the significant wave height. Test B corresponds to longer waves with $kd_{peak} = 0.6$ and $kd_{2fp} = 1.6$, and the degree of non-linearity is considerably higher (S = 54%).

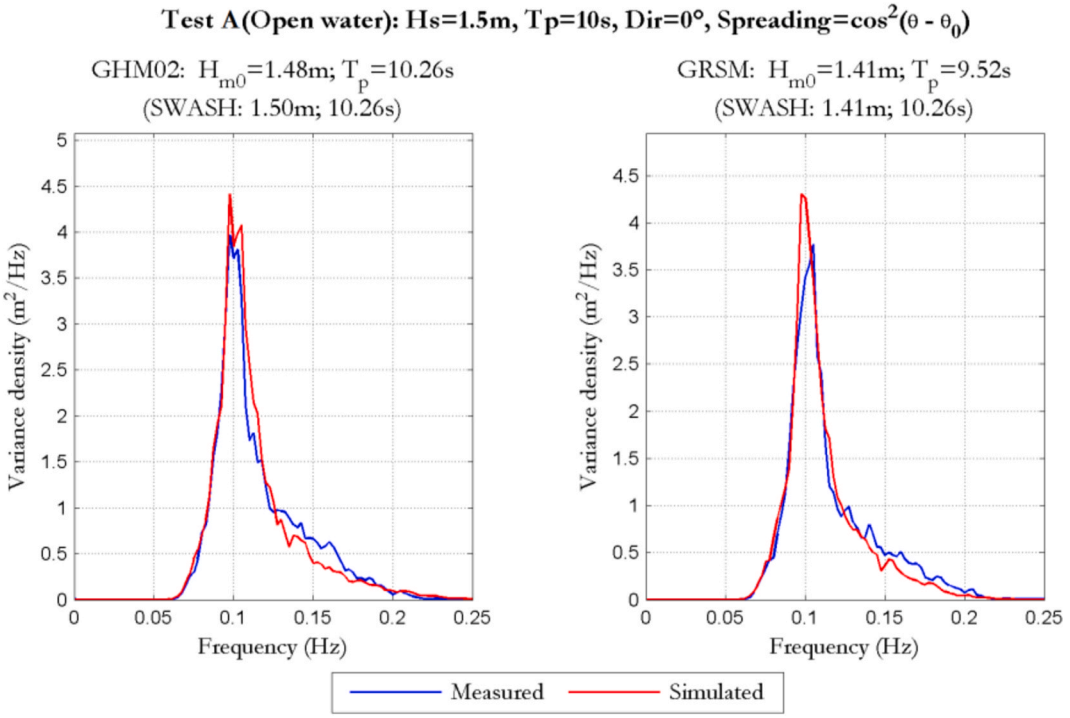

Fig. 8. Measured and simulated wave spectra for Test A.

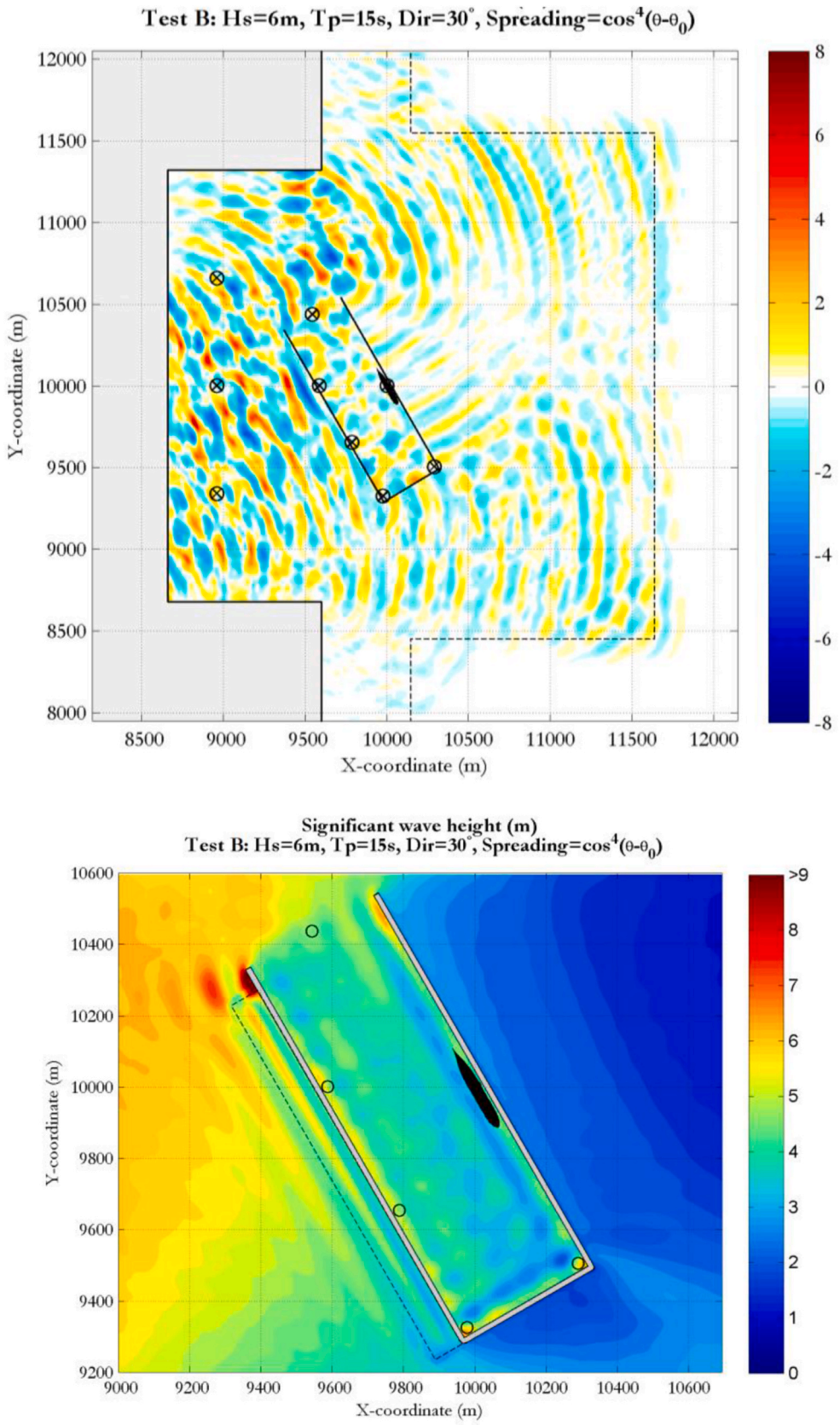

Fig. 9. Snapshot of water level elevation along the domain (top panel) and significant wave height (bottom panel) map for Test B. Circles indicate the location of the wave gauges; the dashed line represents the area of the gravel slope next to the vertical wall of the harbour basin.

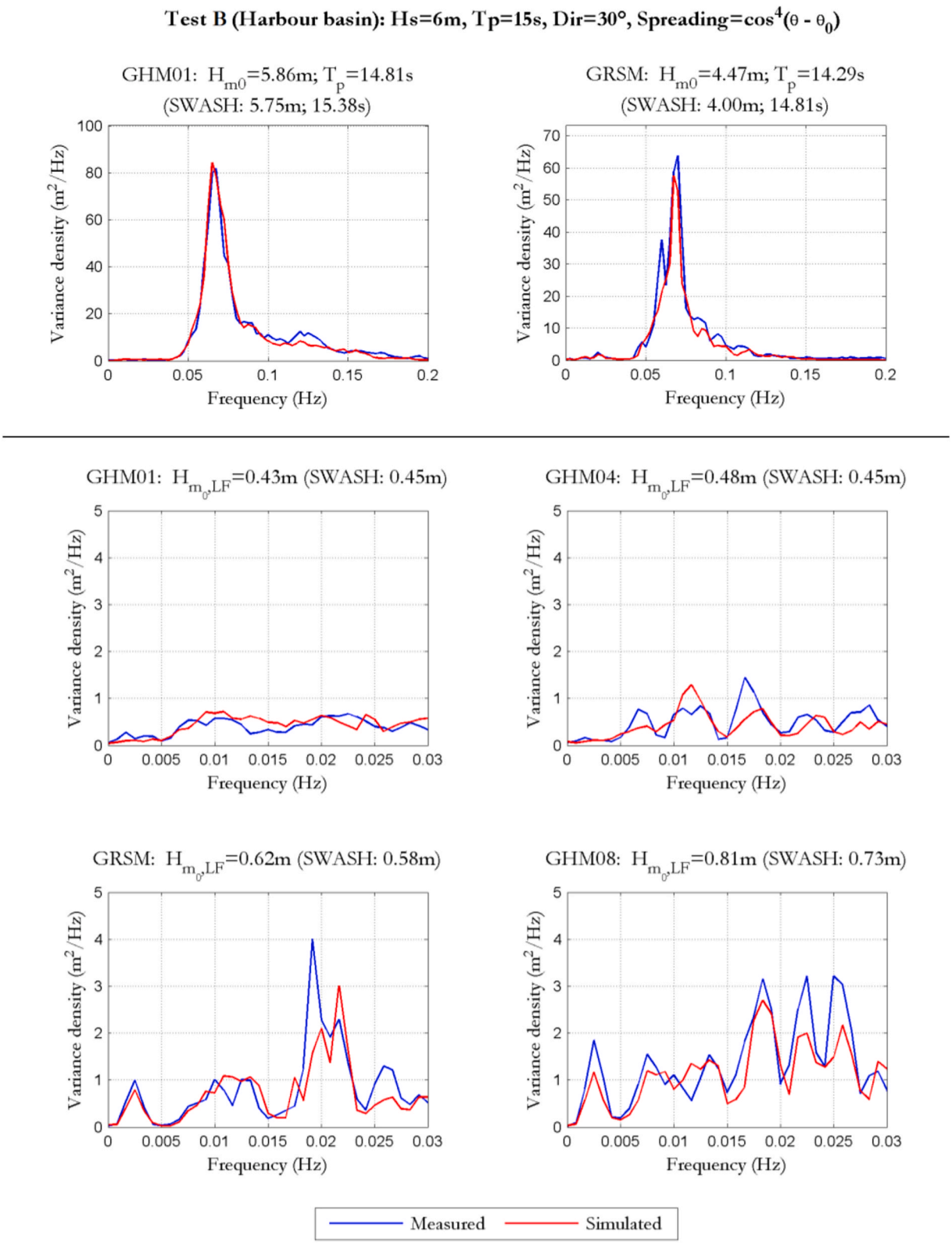

Fig. 10. Measured and simulated wave spectra for Test B. Upper plots: total wave spectra; lower plots: low frequency ($f < 0.03$ Hz) wave spectra.

For both Test A and B the shape and energy levels of the simulated wave spectra correspond well with the measurements, indicating that the model setup and propagation processes are reproduced by the wave model. Following the results of Section 2.1, the slight under estimation at higher frequencies for Test A (Fig. 8) is likely associated with the amplitude errors that take place near the wave model boundary for relatively short waves (i.e., frequency>0.15 Hz and $kd > 2$). The influence of numerical diffusion is expected to be small for these wave components, as the horizontal resolution is reasonable (~16 grid points per wave length) and the associated amplitudes and non-linearity are relatively low.

In Test B waves are relatively long, so amplitude errors near the

boundary are expected to be small. Despite the highly non-linear conditions in Test B, amplitude errors due to numerical diffusion are also small (Fig. 10). This suggests that the provided grid resolution is sufficient for also for higher frequency bands (~20 grid points per wave length for components with frequency = 0.13 Hz).

The comparisons of measured and simulated total significant wave height at the 9 wave gauges indicate maximum differences in the order of 10% for both Test A and B. The overall agreement between the physical scale and numerical models demonstrate that the SWASH model can properly handle extremely energetic waves and complex reflection inducing wave trapping as standing waves into the harbour basin (Figs. 9 and 10).

For Test A the amount of energy in the low frequency bands (wave components with T > 33s) is rather small, corresponding to an $H_{m0,LF}$ of 0.02 m in both the measurements and computations. The performance of the model for Test B with respect to the low frequency waves is noteworthy (lower plots of Fig. 10). The deviations between measured and the simulated low frequency wave heights at the 9 wave gauges are in the order of 10%. The low frequency wave spectra are also in good agreement: outside the harbour basin the wave energy is evenly distributed along the spectra, while inside the harbour the excitation of the seiching modes are noticed as peaks in the measured and simulated low frequency wave spectra.

3.2. Computation of wave forces

The mesh of the Panamax ship representing the modelled vessel used in the Harberth model is displayed in Fig. 11. In Tests B, a quay wall is included as an additional body in the boundary-integral model to account for reflections of the scattered and radiated waves. Incident wave conditions are not prescribed at the quay wall, as the obstacle is already included in the SWASH wave model and therefore in the incident waves. The wall is placed in the starboard side of the ship at 20 m from its centreline. Especially between the ship and the wall, viscous effects are not negligible. To approximate these effects a wall transmission coefficient is applied (ε_t = 0.02), following (Van der Molen, 2006). The selected coefficient represents a smooth quay wall close to the ship. In case of rough structures such as rubble-mound breakwaters a much larger value may be required. Further, viscous damping is usually quadratically related to the wave height, while the transmission coefficient provides a linear reduction of the wave forces. Therefore, different values can be found for different wave conditions. However, the transmission coefficient used in Test B was not specifically tuned for improved results.

The *coupling tool* was used to convert the results of the SWASH simulations into the Harberth model input files. The Harberth simulations were 3 h long and took approximately 5 h of computational time using a conventional laptop. The computed first- and second-order forces and moments were combined for the analysis, as these are measured simultaneously as one resulting time series in the tests. The components of the second-order forces that correspond to corrections due to the motions of the ship are not taken into account in the Harberth computation because the ship is retrained in the model tests. The measured and computed forces and moments acting on the ship of Test A (open water situation) are compared in Table 3 and Fig. 12. Results for Test B (schematic port basin) are given in Table 4 and Fig. 13. To facilitate comparisons, spectral forces and moments are quantified in terms of 'significant force amplitudes':

$$F_{m0} = 2\sqrt{m_0}$$

Where m_0 is the zeroth-order moment (area) of the forces and moments spectra. Significant force amplitudes are quantified for the full spectrum (total) and for the frequency band lower than 0.03 Hz (low frequency).

In general, the computed force and moment spectra agree well with measurements. For Test B, however, the computed moments *Mx* and *Mz* show significant discrepancies as their spectral levels are underpredicted. Overall differences between measured and simulated loads can be attributed to inaccuracies in the simulated wave fields, limitations intrinsic to the Harberth model, the untuned wall transmission coefficient used in the Harberth computations (Test B) and the precision of the measurements (transducers and set-up applied). The slight underestimation of the simulated wave height at the location of the ship quoted in the caption of Tables 3 and 4 partially explain the deviations on total and low frequency forces.

Especially for Test A, where the low frequency waves are minor, the relative differences in the low frequency forces correspond to small absolute errors that are likely influenced by the accuracy of the force transducers. Differences in the 'roll moments' (*Mx*) are ascribed to the method applied in the tests to derive this parameter from the measured pressure transducers signals. *Mx* is calculated based on the difference between two signals with relatively high readings; therefore, a small measurement error in one of the probes can result in a relatively large error in the value for roll (De Jong et al., 2005). For this reason, 'roll moments' (*Mx*) are known to be difficult to measure accurately on restraint model vessels. Moreover, similar differences in the 'yaw moments' (*Mz*) were found by (Rijnsdorp and Zijlema, 2016; Van der Molen, 2006; Van Der Molen et al., 2006; Van der Molen and Wenneker, 2008), who used data from the same experiment and computed the wave forces using distinct computational approaches. Hence, the reported deviations in *Mx* and *Mz* are likely be related to the difficulties in measuring moments that act on a restrained ship, but also limitations of the computational tools to represent the specific test condition.

It must be highlighted that Test B represents an extremely energetic condition, with significant wave height in the order of 6 m outside the harbour and 4 m inside the harbour, exceeding by far the most severe conditions expected at mooring locations. Still, the developed approach produced reasonably accurate results. The SWASH model was able to cope with the extreme wave conditions in terms of numerical stability and accuracy, reproducing the complex wave field inside the harbour associated with the reflection of short and infragravity waves (see Figs. 9 and 10). The coupling tool effectively transferred the wave information from SWASH to Harberth, and the Harberth model was able to replicate the exceptional loads under such highly non-linear conditions.

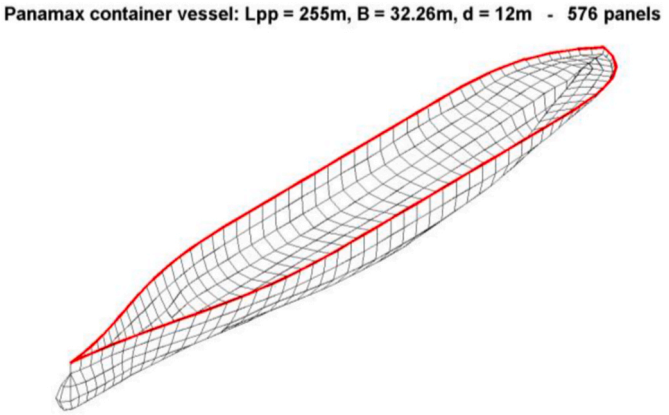

Fig. 11. Panel description of the Panamax container vessel (576 panels and 104 water line segments).

4. Conclusions

The wave model SWASH and the Harberth model have been successfully coupled for assessing wave forcing on moored ships in complex port geometries. The SWASH model can reproduce accurately the relevant processes involved in wave penetration, provided that the computational grid has sufficient resolution, otherwise numerical dissipation can be detrimental to the outcomes. As a general indication,

Table 3
Measured and simulated 'significant force amplitudes': Test A. $F_{m0} = 2(m_0)^{0.5}$; Low-frequency band: f < 0.03Hz. Deviations in the simulated wave height at the location of the ship: $\Delta Hs_{total} = -0.1\%$; $\Delta Hs_{LF} = -7.5\%$.

Mode	Fm_0 (total)			Fm_0 (low frequency)		
	Measured	Simulated	%	Measured	Simulated	%
Fx [MN]	1.76	1.60	−9.2	0.06	0.08	35.1
Fy [MN]	11.73	11.96	2.0	0.22	0.30	38.6
Fz [MN]	13.94	16.43	17.9	0.47	0.46	−1.7
Mx [MNm]	24.01	23.83	−0.8	3.14	0.69	−77.9
My [MNm]	788.71	749.38	−5.0	12.82	19.60	52.9
Mz [MNm]	707.83	513.09	−27.5	10.51	20.84	98.2

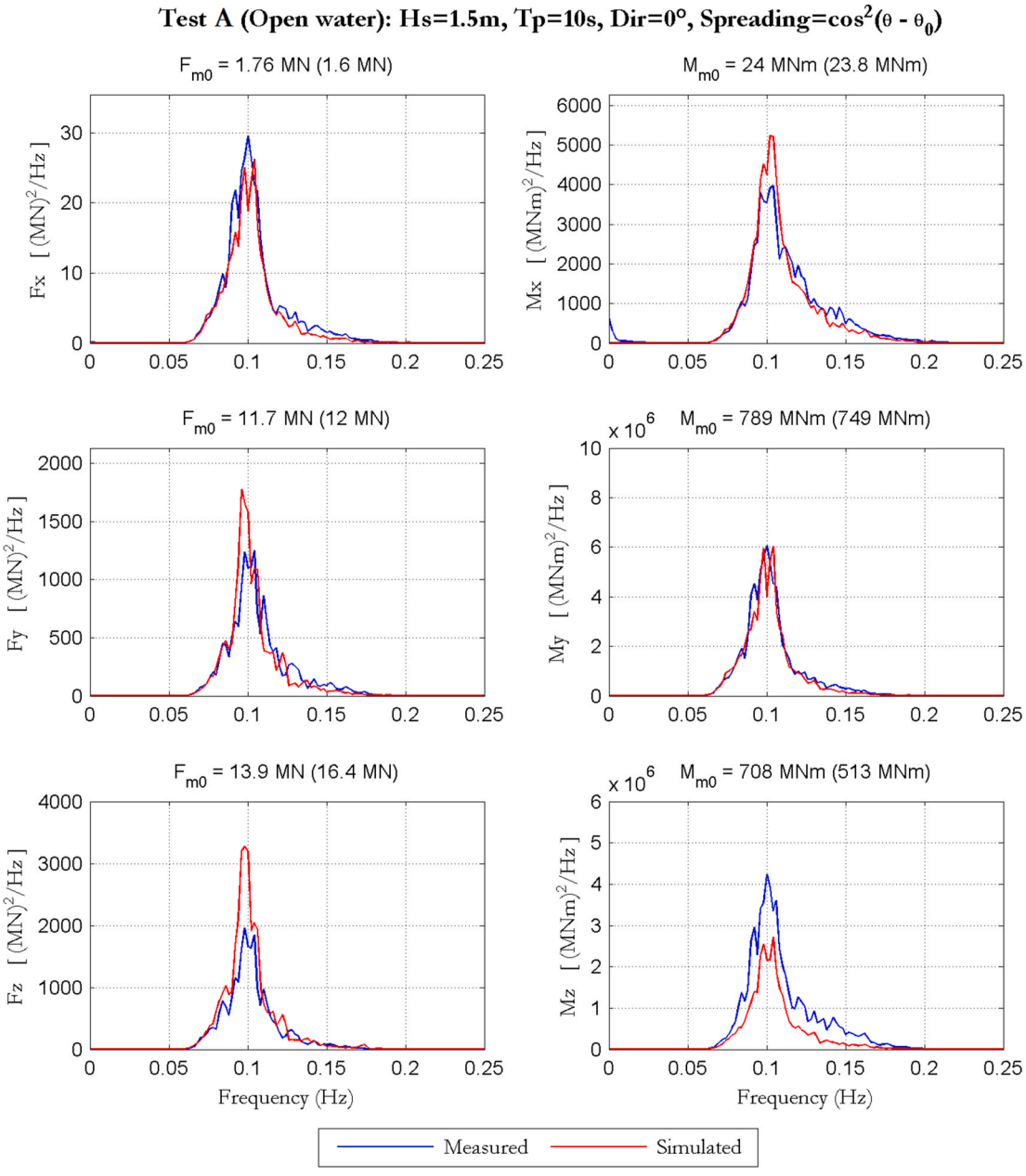

Fig. 12. Measured and simulated spectra of forces and moments of Test A.

two vertical layers are sufficient and the horizontal grid spacing should be in the order of 30–40 grid points per wave length associated with the peak period (λ_{tp}), so that the higher frequency wave components are still properly modelled. For instance, considering $\lambda_{tp}/\lambda_{0.5*tp} \approx 2.5$, the resolution for wave components with twice the peak frequency is still in the order of 15 grid points per wave length. As computational times are strongly related to the grid resolution, this requirement for accuracy may have practical implications especially for applications involving large areas relative to the typical wave lengths. In such cases, acceptable computation times may be achieved by further optimizing grid

Table 4
Measured and simulated 'significant force amplitudes': Test B. $F_{m0} = 2(m_0)^{0.5}$; Low-frequency band: f < 0.03Hz. Deviations in the simulated wave height at the location of the ship: $\Delta Hs_{total} = -10.5\%$; $\Delta Hs_{LF} = -7.2\%$.

Mode	Fm_0 (total)			Fm_0 (low frequency)		
	Measured	Simulated	%	Measured	Simulated	%
Fx [MN]	9.63	8.03	−16.6	1.20	1.05	−12.4
Fy [MN]	35.94	31.43	−12.6	2.13	1.78	−16.3
Fz [MN]	92.43	86.72	−6.2	17.66	16.79	−4.9
Mx [MNm]	119.49	52.43	−56.1	25.45	3.35	−86.9
My [MNm]	4 178.86	3 588.40	−14.1	492.63	423.40	−14.1
Mz [MNm]	2 141.08	1 350.01	−36.9	121.45	82.72	−31.9

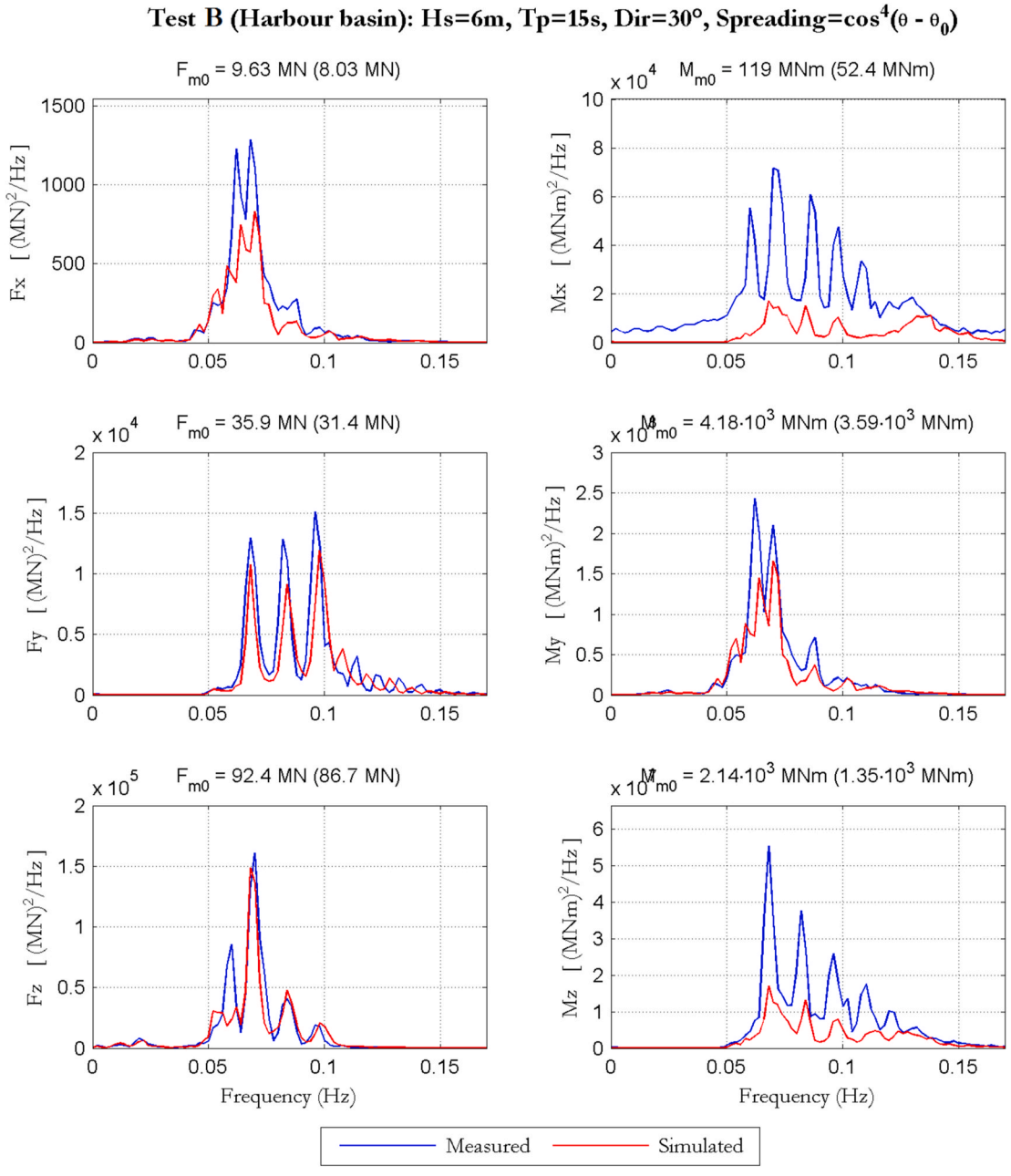

Fig. 13. Measured and simulated spectra of forces and moments of Test B.

resolution (e.g., use of unstructured meshes) and/or reducing the domain of simulation. The required wall clock time can also be reduced by applying the parallel version of SWASH and using multiple computational cores (e.g., cluster), so that the model performance is effectively scaled.

The numerical tests with shorter regular waves ($kd > 1$) indicated considerable numerical dissipation along the domain, which was minimized by enforcing momentum conservation and using a higher-order

numerical scheme for the vertical advection of u-momentum (i.e., using the *adapted* set of schemes).

The overall approach used for wave generation in SWASH results in a wave energy drop near the model boundary for relatively short waves ($kd \geq 3$). In applications where such shorter waves are relevant, these near-boundary amplitude errors can be compensated by amplifying the imposed wave spectra at the higher frequencies. Further, especially for strongly non-linear conditions (e.g., large waves in shallow water) spurious high-frequency waves might be introduced in the incoming boundary due to the omission of super harmonics in the numerical wave maker of SWASH. Improving the wave generation in SWASH is outside of the scope of the present study and may be subject to future research and developments for accuracy over a wider range of conditions by means of, e.g., internal wave generation techniques and higher-order boundary conditions accounting for super harmonics.

The novel coupling strategy developed in this paper to combine the SWASH and Harberth models attested to be accurate and robust. The approach may impose additional requirements in applications where shorter waves ($kd > 3$) are primarily relevant for the 1st order forces, vessel motions and drift forces – which is typically not the case in shallower coastal areas. Then, additional vertical layers should be used in SWASH simulations in order to properly prescribe the vertical profiles of incident waves along the ship hull. Finally, the wave forces and moments acting on a moored ship were effectively determined by the Harberth model based on the computed wave information at and around the location of the ship.

The proposed methodology for computing the wave loads on moored vessels (SWASH + *coupling tool* + Harberth) demonstrated satisfactory performance for the validation tests, which included extreme wave conditions (Hs $\approx$ 6m, $H_{m0,LF} \approx$ 0.8m) propagating in intermediate/shallow waters and influenced by a schematic port geometry, where complex and non-linear shallow water processes are relevant to define the wave field at a mooring location. Under such conditions, the developed approach can be applied for the design of new ports and for assessments of mooring problems in existing terminals.

CRediT authorship contribution statement

João P.H. Dobrochinski: Methodology, Formal analysis, Investigation, Writing – original draft. **Alex van Deyzen:** Conceptualization, Methodology, Resources, Writing – review & editing. **Marcel Zijlema:** Methodology, Software, Writing – review & editing. **Arne van der Hout:** Methodology, Writing – review & editing.

Declaration of competing interest

The authors declare that they have no known competing financial interests or personal relationships that could have appeared to influence the work reported in this paper.

Data availability

The authors do not have permission to share data.

Acknowledgements

This study was part of the MSc thesis of the first author João P.H. Dobrochinski (TU Delft/Hydraulic Engineering, Netherlands), and was supported by Royal Haskoning-DHV. The project was developed as a joint research between RHDHV, TU Delft and Deltares (Netherlands). The authors would like to thank Prof. Tiedo Vellinga (TU Delft), Bas Wijdeven (TU Delft/RHDHV), and Cock van der Lem (RHDHV) for their key guidance and motivation during the study. The contributions of Wim van der Molen in assisting with the Harberth simulations, providing the Wavescat results for comparison, and reviewing the paper manuscript are greatly appreciated. We would also like to thank Martijn de Jong for the valuable inputs while reviewing the manuscript. Finally, Deltares is acknowledged for providing the model test data used in the model validation.

References

Bingham, H.B., 2000. A hybrid Boussinesq-panel method for predicting the motion of a moored ship. Coast. Eng. 40, 21–38.

Christensen, E.D., Jensen, B., Mortensen, S.B., Hansen, H.F., Kirkegaard, J., 2008. Numerical simulation of ship motion in offshore and harbour areas. In: Proceedings 27th OMAE. Estoril, Portugal.

De Jong, M.P.C., Weiler, O.M., Borsboom, M.J.A., Van Dongeren, A.R., 2005. A Phase-Resolving Analysis Technique for Short-Crested Wave Fields. Proceedings 5th International Symposium WAVES, Madrid, Spain.

De Jong, M.P.C., Borsboom, M.J.A., Dekker, J., 2009. Calculation of Low-Frequency Waves in Shallow Water and Comparison to Common Practice in Diffraction Methods. Proceedings 28th OMAE, Honolulu, HI, USA.

De Jong, M.P.C., de Bont, J.A.M., Borsboom, M., Van Vossen, B., 2011. Evaluation of an Extended Operational Boussinesq-type Wave Model for Calculating Low-Frequency Waves in Intermediate Depths. Proceedings 30th OMAE, Rotterdam, The Netherlands.

De Roo, S., Suzuki, T., Kolokythas, G., Zhao, G., Verwaest, T., 2015. Numerical Modelling of 2D Wave Transformation Processes from Nearshore to a Shallow Foreshore: Comparison between the Mike21, SWASH and XBEACH Models. IAHR, The Hague, The Netherlands.

Dobrochinski, J.P.H., 2014. A Combination of SWASH and Harberth to Compute Wave Forces on Moored Ships. MSc Thesis, Delft University of Technology, Delft, The Netherlands. https://repository.tudelft.nl/islandora/object/uuid:a0b269f8-6dc3-4de0-b1bd-918577f1456f.

Fenton, J.D., 1990. Nonlinear wave theories. In: Le Mehaute, B., Hanes, D.M. (Eds.), The Sea, Ocean Engineering Science, vol. 9. John Wiley & Sons, New York, USA, pp. 3–25.

Hirsch, C., 1990. Numerical Computation of Internal and External Flows. In: Fundamentals of Numerical Discretization, vol. 1. John Wiley and Sons, Chichester.

Hughes, S.A., 1993. Physical Models and Laboratory Techniques in Coastal Engineering. World Scientific, Singapore.

Hydraulics, WL|Delft, 2004. Projectbeschrijving R&D Havens EZ-LIP: H3896.40 Validatie Golfkrachten Op Schepen (Validation Wave Forces on Ships). Delft, The Netherlands (in Dutch).

Jaouën, F., Waals, O., de Jong, M.P.C., Van der Hout, A.J., Christou, M., 2016. Methodology for the design of LNG terminals in a nearshore environment. In: Proceedings 35th OMAE, Busan, South Korea.

Mynett, A.E., Keuning, P.J., Vis, F.C., 1985. The Dynamic Behaviour of Moored Vessels inside a Harbour Configuration. Birmingham, England, p. 10.

Naciri, M., Sergent, E., 2009. *Diffraction/radiation of 135,000m^3 Storage Capacity LNG Carrier in Shallow Water – a Benchmark Study*. Proceedings 28th OMAE, Honolulu, Hawaii, USA.

Permanent International Association of Navigation Congresses – Pianc, 1995. In: Working Group 24: Criteria for Movements of Moored Ships in Harbours.

Permanent International Association of Navigation Congresses – Pianc, 2012. Working Group 115: *Criteria For the (Un)loading of Container Vessels*.

Reniers, A.J.H.M., Roelvink, J.A., Thornton, E.B., 2004. Morphodynamic modeling of an embayed beach under wave group forcing. J. Geophys. Res. 109, C01030 https://doi.org/10.1029/2002JC001586.

Rijnsdorp, D.P., Zijlema, M., 2016. Simulating waves and their interactions with a restrained ship using a non-hydrostatic wave-flow model. Coast Eng. 114, 119–136.

Rijnsdorp, D.P., Smit, P.B., Zijlema, M., 2014. Non-hydrostatic modelling of infragravity waves under laboratory conditions. Coast Eng. 85, 30–42.

Smit, P.B., Zijlema, M., Stelling, G.S., 2013. Depth-induced wave breaking in a nonhydrostatic, near-shore wave model. Coast. Eng. 76, 1–16.

Van der Hout, A.J., De Jong, M.P.C., Jaouën, F., Waals, O.J., 2015. Long Waves in Intermediate Depths and Their Influence on the Design of Nearshore Terminals. IAHR, The Hague, The Netherlands.

Van der Molen, W., 2006. Behaviour of Moored Ships in Harbours. PhD Thesis. Delft University of Technology, Delft, The Netherlands.

Van der Molen, W., 2011. Boundary Element Model Wavescat: Description and Validation. CSIR Report.

Van der Molen, W., Wenneker, I., 2008. Time-domain calculation of moored ship motions in nonlinear waves. Coast Eng. 55, 409–422. https://doi.org/10.1016/j.coastaleng.2008.01.001.

Van Der Molen, W., Monárdez, P., Van Dongeren, A.R., 2006. Numerical simulation of long period-waves and ship motions in Tomakomai port, Japan. Coast Eng. J. 48 (1), 56–59.

Van der Molen, W., Rossouw, M., Phelp, D., Tulsi, K., Terblanche, L., 2010. Innovative technologies to accurately model waves and moored ship motions. In: Science Real and Relevant Conference. CSIR.

Van der Molen, W., Thomson, G., Nitkin, J., Taylor, D., Scott, D., 2019. Forecasting Squat of Post Panamax Container Ships in PortMiami's Entrance Channel. Ports'19 Conf., Pittsburgh, PA, USA.

Van Dongeren, A.R., Klopman, G., Reniers, A.J.H.M., Petit, H.A.H., 2001. High quality laboratory wave generation for flumes and basins. In: Proc. WAVES, vol. 2. San Francisco, CA, pp. 1190–1199.

Van Mierlo, F.A.J.M., 2014. Numerical Modelling of Wave Penetration in Ports. MSc Thesis, Delft University of Technology, Delft, The Netherlands.

Vasarmidis, P., Stratigaki, V., Suzuki, T., Zijlema, M., Troch, P., 2019. Internal wave generation in a non-hydrostatic wave model. Water 11, 986. https://doi.org/10.3390/w11050986.

Vasarmidis, P., Stratigaki, V., Suzuki, T., Zijlema, M., Troch, P., 2021. On the accuracy of internal wave generation method in a non-hydrostatic wave model to generate and absorb dispersive and directional waves. Ocean Eng. 219, 108303 https://doi.org/10.1016/j.oceaneng.2020.108303.

Wenneker, I., Borsboom, M.J.A., Pinkster, J.A., Weiler, O.M., 2006. A Boussinesq-type wave model coupled to a diffraction model to simulate wave-induced ship motion. In: Proceedings of the 31st PIANC World Congress. Estoril, Portugal.

Zijlema, M., 2019. The role of the Rankine-Hugoniot relations in staggered finite difference schemes for the shallow water equations. Comput. Fluids 192. https://doi.org/10.1016/j.compfluid.2019.104274 article 104274.

Zijlema, M., Stelling, G.S., 2005. Further experiences with computing non-hydrostatic free-surface flows involving water waves. Int. J. Numer. Methods Fluid. 48, 169–197.

Zijlema, M., Stelling, G., Smit, P., 2011. SWASH: an operational public domain code for simulating wave fields and rapidly varied flows in coastal waters. Coast Eng. 58, 992–1012. https://doi.org/10.1016/j.coastaleng.2011.05.015.